

This is an Open Access document downloaded from ORCA, Cardiff University's institutional repository:<https://orca.cardiff.ac.uk/id/eprint/163368/>

This is the author's version of a work that was submitted to / accepted for publication.

Citation for final published version:

Wang, Qiaoyun, Maramizonouz, Sadaf, Stringer Martin, Mercedes, Zhang, Jikai, Ong, Hui Ling, Liu, Qiang, Yang, Xin, Rahmati, Mohammad, Torun, Hamdi, Ng, Wai Pang, Wu, Qiang, Binns, Richard and Fu, Yongqing 2024. Acoustofluidic patterning in glass capillaries using travelling acoustic waves based on thin film flexible platform. *Ultrasonics* 136, 107149. 10.1016/j.ultras.2023.107149

Publishers page: <http://dx.doi.org/10.1016/j.ultras.2023.107149>

Please note:

Changes made as a result of publishing processes such as copy-editing, formatting and page numbers may not be reflected in this version. For the definitive version of this publication, please refer to the published source. You are advised to consult the publisher's version if you wish to cite this paper.

This version is being made available in accordance with publisher policies. See <http://orca.cf.ac.uk/policies.html> for usage policies. Copyright and moral rights for publications made available in ORCA are retained by the copyright holders.



# **Acoustofluidic Patterning in Glass Capillaries Using Travelling Acoustic waves based on Thin Film Flexible Platform**

Qiaoyun Wang<sup>1,2</sup>, Sadaf Maramizonouz<sup>3,2</sup>, Mercedes Stringer Martin<sup>4</sup>, Jikai Zhang<sup>2</sup>, Hui Ling Ong<sup>2</sup>, Qiang Liu<sup>1,2</sup>, Xin Yang<sup>4</sup>, Mohammad Rahmati<sup>2</sup>, Hamdi Torun<sup>2</sup>, Wai Pang Ng<sup>2</sup>, Qiang Wu<sup>2</sup>, Richard Binns<sup>2</sup>, Yongqing Fu<sup>2,\*</sup>

<sup>1</sup> Hebei Key Laboratory of Micro-Nano Precision Optical Sensing and Measurement Technology, School of Control Engineering, Northeastern University at Qinhuangdao, 066004, P.R. China

<sup>2</sup> Faculty of Engineering and Environment, Northumbria University, Newcastle upon Tyne, NE1 8ST, UK

<sup>3</sup> School of Engineering, Newcastle University, Newcastle upon Tyne, NE1 7RU, UK

<sup>4</sup> Department of Electrical and Electronic Engineering, School of Engineering, Cardiff University, Cardiff, CF24 3AA, UK

\*Corresponding authors: Professor Richard YongQing Fu, E-mail: richard.fu@northumbria.ac.uk

## **Abstract**

Surface acoustic wave (SAW) technology has been widely used to manipulate microparticles and biological species, based on acoustic radiation force (ARF) and drag force induced by acoustic streaming, either by standing SAWs (SSAWs) or travelling SAWs (TSAWs). These acoustofluidic patterning functions can be achieved within a polymer chamber or a glass capillary with various cross-sections positioned along the wave propagating paths. In this paper, we demonstrated that microparticles can be aligned, patterned, and concentrated within both circular and rectangular glass capillaries using TSAWs based on a piezoelectric thin film acoustic wave platform. The glass capillary was placed at different angles along with the interdigital transducer directions. We systematically investigated effects of tilting angles and wave

characteristics using numerical simulations in both circular and square shaped capillaries, and the patterning mechanisms were discussed and compared with those agitated under the SSAWs. We then experimentally verified the particle patterns within different glass capillaries using thin film ZnO SAW devices on aluminum (Al) sheets. Results show that the propagating SAWs can generate acoustic pressures and patterns in the fluid due to the diffractive effects, drag forces and ARF, as functions of the SAW device's resonant frequency and tilting angle. We demonstrated potential applications using this multiplexing, integrated, and flexible thin film-based platform, including patterning particles (1) inside multiple and successively positioned circular tubes; (2) inside a solidified hydrogel in the glass capillary; and (3) by wrapping a flexible ZnO/Al SAW device around the glass capillary.

**Keywords:** Surface acoustic wave, acoustofluidics, glass capillary, patterning

## 1. Introduction

Acoustofluidic devices have been widely used for biosensing and manipulation of particles and biological species in lab-on-chip and point-of-care applications [1, 2]. Acoustofluidic manipulation is generally achieved using transducers that convert electrical energy into mechanical vibrations and generate sound waves in the fluid channels or directly in liquid droplets. For example, piezoelectric transducers plates can be used to generate bulk acoustic waves (BAWs) inside a channel for manipulations, or interdigital transducers (IDTs) can be used to generate surface acoustic waves (SAWs) along the surface of the material for patterning. Compared with the BAW devices, SAW technology offers remote and precise control, biocompatibility, low energy requirements, multiple modes, miniature size and simple designs [3]. SAW devices are versatile and flexible, and can generate different patterns for different purposes whilst being non-invasive, label-free, low power consumption and high biocompatibility [4-7].

Manipulation using SAWs can be realized by either using two opposing SAWs that interfere with each other to generate standing SAWs (SSAWs) [3, 5, 8-12], by using a

traveling SAWs (TSAWs) propagating in one direction [4], or by using a combination of both of these waves such as in multi-stage devices [13, 14]. SSAW-based manipulation typically relies on the generation of acoustic radiation forces (ARFs) to actuate objects toward the generated nodes and anti-nodes [15-18], for separating blood components and isolation of circulating tumor cells [19] and cancer cells [20], bacteria [21] and other biological cells [22-25]. However, the patterns generated by SSAWs are often restricted to half-wavelength periodic distances between nodes or anti-nodes. SSAWs are often used to manipulate micro-sized particles because the acoustic radiation force is decreased with particle sizes [26, 27].

On the other hand, TSAWs can also achieve particle manipulation functions based on two effects, i.e., (1) drifting caused by acoustic streaming and the induced drag force; and (2) the particles' movements caused by the ARFs [28]. The TSAWs have the advantages of high spatial resolution and precise alignment, less restriction on the alignment and channel resonance [26], and no inherent displacement limit of the half wavelength compared with methods based on standing acoustic field [29]. Therefore, they permit manipulation of both microscale objects and sub-micrometer objects. This allows multiple biological applications such as nanoscale manipulation [30], and separation [31] or exosome enrichment [32].

Most SSAW or TSAW microfluidic devices use PDMS microchannels with rectangular cross-sections [30-32], due to their ease of fabrication and integration. However, PDMS does not have good acoustic transmission and reflection performance [4], and they also have issues with complicated fabrication, alignment, bonding, and difficulties in the adjustment of the bonded microchannels [26]. Alternatively, glass capillaries offer effective acoustic transmission, low acoustic attenuation and large differences in acoustic impedance compared with the fluid [33], thus allowing for effective propagation of acoustic waves and strong lateral acoustic resonances [33]. Additionally, glass capillaries allow flexibility in their channel designs (e.g., mass manufactured circular, square, and rectangular ones [34]), excellent optical transparency, no additional bonding of various acoustofluidic components, and good re-adjustment and disposability [33, 34], making them ideal materials for acoustofluidic

channels. Glass capillary tubes have already been incorporated with acoustic devices to manipulate microparticles and biological cells [33, 34].

Several studies of acoustofluidic manipulations have been published using the BAW and glass capillaries [33]. Nevertheless, only a few studies have been performed using SAWs for particle manipulation in glass capillaries [34, 35]. For example, Lata *et al.* [35] used SSAWs and a coupling layer technique to pattern cells inside a square-shaped glass capillary tube along with a polyethylene tubing. When the tube was positioned perpendicular or parallel to the IDTs, the particles will be patterned perpendicular or parallel to the incident waves, respectively. Their results showed that perpendicular alignment created repeating clusters of micro-objects with a distance of  $\frac{1}{2}$  SAW wavelength, while parallel alignment created straight lines of micro-objects with a distance of 1 cm. They were able to mimic physiological cell patterning in tissues in a 3D manner whilst maintaining a high spatial resolution. Maramizonouz *et al.* [34] investigated microparticle patterning inside both rectangular and circular glass capillaries using the SSAWs and studied the influences of tube configuration and tilting angle, which have been illustrated in **Fig. 1** (a) and (b). Results demonstrated that there are two types of generated patterns, in which the patterning at the bottom of the tube is parallel to the tube direction with different angles in relation to the IDTs, but the patterning in the middle of the tube is perpendicular to the tube direction [24]. Additionally, they demonstrated the use of glass capillary tubes with flexible thin film SAW devices. Flexible thin film SAW devices [36] are beneficial due to their easy integration with other microelectronic technologies [37, 38], and easy applications in flexible microfluidic platform, body conforming wearable devices, and soft robotics [34, 38].

Well-patterned acoustic fields have been shown to generate in the glass capillaries using the SSAW devices, and their distances between the nodes are restricted to half-wavelength [26, 39]. In contrast, TSAW has advantages such as high spatial resolution and less restriction on the alignment patterns. Compared with SSAWs, TSAWs produced by IDTs from one side of the microchannel will push the particles along the acoustic propagation direction by the radiation forces, as shown in **Figs. 1** (c) and (d)

[40, 41]. Studies about the applications of fluid flow and particle migration using the TSAW have been reported over the past decades [42-44]. For example, Mao *et al.* [45] used a chirped SAW device to generate a single vortex acoustic streaming in a square glass capillary to enrich sub-micrometer and nanometer-sized particles (80 to 500 nm). Destgeer *et al.* [46] reported to use high frequency (133 MHz) TSAWs and separate both the 3  $\mu\text{m}$  and 10  $\mu\text{m}$  particles in the PDMS channels with a high separation efficiency of nearly 100%. Collins *et al.* [40] investigated effects of particle focusing in the PDMS channels using the TSAWs with a frequency of 633 MHz. Ma *et al.* [47] separated 15.2  $\mu\text{m}$  particles from 10.2 and 8  $\mu\text{m}$  particles using TSAW devices with a frequency of 45.52 MHz, and achieved a high efficiency of  $\sim 92\%$ .

Recently there are some papers about particle patterning using the TSAWs within rectangular glass capillaries [34, 48], but few studies have been done using TSAWs within circular glass capillaries. In this paper, we systematically studied the generation of microparticle patterns inside circular glass capillaries actuated using the TSAWs and compared with those using the SSAWs, both of which are illustrated in **Fig. 1**. Acoustic waves and pressure patterns generated inside both the circular and rectangular capillaries were investigated as results of agitation due to the propagating acoustic waves into the glass tubes through both simulations and experimental studies. Microparticle patterns generated inside glass capillaries have been systematically studied at different SAW frequencies, cross-sections (both rectangular and circular) and diameters of glass capillaries, as well as different tilting angles of capillaries relate to the IDTs direction. Finally, their potential applications in different scenarios were explored. This work is focused on particle manipulation in glass capillaries using travelling acoustomechanical waves, and circular capillaries are especially important as they are abundant in biological systems including blood vessels. The acoustomechanical transducers in this work are flexible and can be wrapped around circular capillaries for additional capabilities.

## **2 Capillary acoustofluidics: design methodologies and simulations**

### **2.1. Design methodologies**

In this study, both the circular glass capillary (with two outer diameter or OD sizes OD= 1.0 mm and OD=550  $\mu\text{m}$ , and length of  $\sim 20$  mm) and the rectangular glass capillary (width 2.3 mm and height 0.5 mm, and length of 20 mm) were used. The mixture suspension of polystyrene (PS) microparticles (Sigma-Aldrich, 79166, with 3  $\mu\text{m}$  diameter and a density of 1900  $\text{kg}/\text{m}^3$ ) and deionized (DI) water was used. The mixtures were then injected using a syringe into the capillary. The glass capillary was placed on the surface of the SAW device. To improve the efficiency of acoustic coupling, a droplet of DI water (about 1.0  $\mu\text{L}$ ) was placed between the circular glass capillary tube and SAW device, and the DI water filled up the gap between the circular glass capillary and the SAW device according to the capillarity phenomenon. In this design, the wave energy can be effectively transferred from the substrate into the glass capillary.

SAW devices based on piezoelectric thin film materials such as ZnO could be seamlessly integrated into a single lab-on-chip (LOC) device at a low cost [1]. SAW device made on the aluminum (Al) thin sheet or foil substrates has the potential to be used as wearable devices for point-of-care, clinical and biomedical applications for collecting, manipulating, and investigating bodily fluids [1,38]. In this paper, the SAW devices were fabricated on the aluminum (Al) substrate (including Al plate with a thickness of 200  $\mu\text{m}$  or Al foil with a thickness of 50  $\mu\text{m}$ ). ZnO thin film (with a thickness of  $\sim 5$   $\mu\text{m}$ ) was deposited onto Al substrates using a magnetron sputter (Nordiko NS3750) [1]. The IDTs (made from 20/100 nm thick of Cr/Au) were fabricated on the film coated Al plates using a standard photolithography and lift-off process [1]. Firstly, the reflection spectra ( $S_{11}$  scattering parameters) and the acoustic resonant frequency of the IDTs were measured using a network analyzer (Keysight, FieldFox N9913A). The resonant frequencies of the SAW devices used in our experiments were around 6.05, 13.15, and 27.37 MHz (with the SAW IDTs wavelengths about 300, 160 and 80  $\mu\text{m}$ ).

The experimental setup as illustrated in the supporting information **Fig. S1**, was composed of an RF signal generator, a power amplifier, a SAW device, an acoustofluidic system and a microscope. For the experimental work, a sinusoidal signal was generated from a radio frequency (RF) signal generator (AIM-TTI Instruments

TG5011A) and amplified using an RF amplifier (Amplifier Research 75A) before being applied to the IDTs of the SAW device. A video camera (IDS, UI-3880CP-C-HQ-R2, Photron UX50) was used to observe and record the motion of microparticles during the experiments. The detailed set-up and patterns generated in a glass capillary using the SSAWs are shown in **Figs. 1** (a-1), and (b-1), which have been reported in a previous paper [34]. When two SAWs (SAW1 and SAW2) with the same frequencies and amplitudes are propagating in opposite directions, they interfere to form standing SAWs. Then the standing SAWs will be transformed into BAW and radiated into the capillary through the water layer at the SAW device/glass tube interfaces, and the acoustic field is generated inside the capillary, as shown in **Figs. 1** (a-2) and (b-2) [34]. The microparticles suspended in the liquid were activated to move to the acoustic pressure nodes due to the ARF generated [49, 50]. Cross-section illustrations of the capillary structure are shown in **Figs. 1** (a-2) and (b-2), respectively. The details can be found in Ref. [34].

The schematic illustration of a TSAWs system with a capillary is shown in **Figs. 1** (c-1) and (d-1). The cross-section illustrations of the capillary structure are shown in **Figs. 1** (c-2) and (d-2), respectively. For the circular patterns (shown in **Fig. 1** (c-1)), the TSAWs are propagated along the substrate and radiated into the DI water to form a leaky SAW. The Huygens–Fresnel principle [7] can be used to explain the patterning effect in the capillary with the TSAWs. The acoustic field magnitude in the capillary is the sum of the contributions from the wave sources. The SAWs propagated in the substrate and DI water have different path lengths, sound speed and phases. The capillary wall will generate the diffractive effect, and the interaction between substrate wavefronts and the fluid wavefront will produce a periodic acoustic field within the circular glass capillary [26]. The microparticles inside the circular glass capillary will be pushed by ARF and streaming-induced drag forces, which form interference patterns on the microparticles, as shown in **Fig. 1** (c-2).

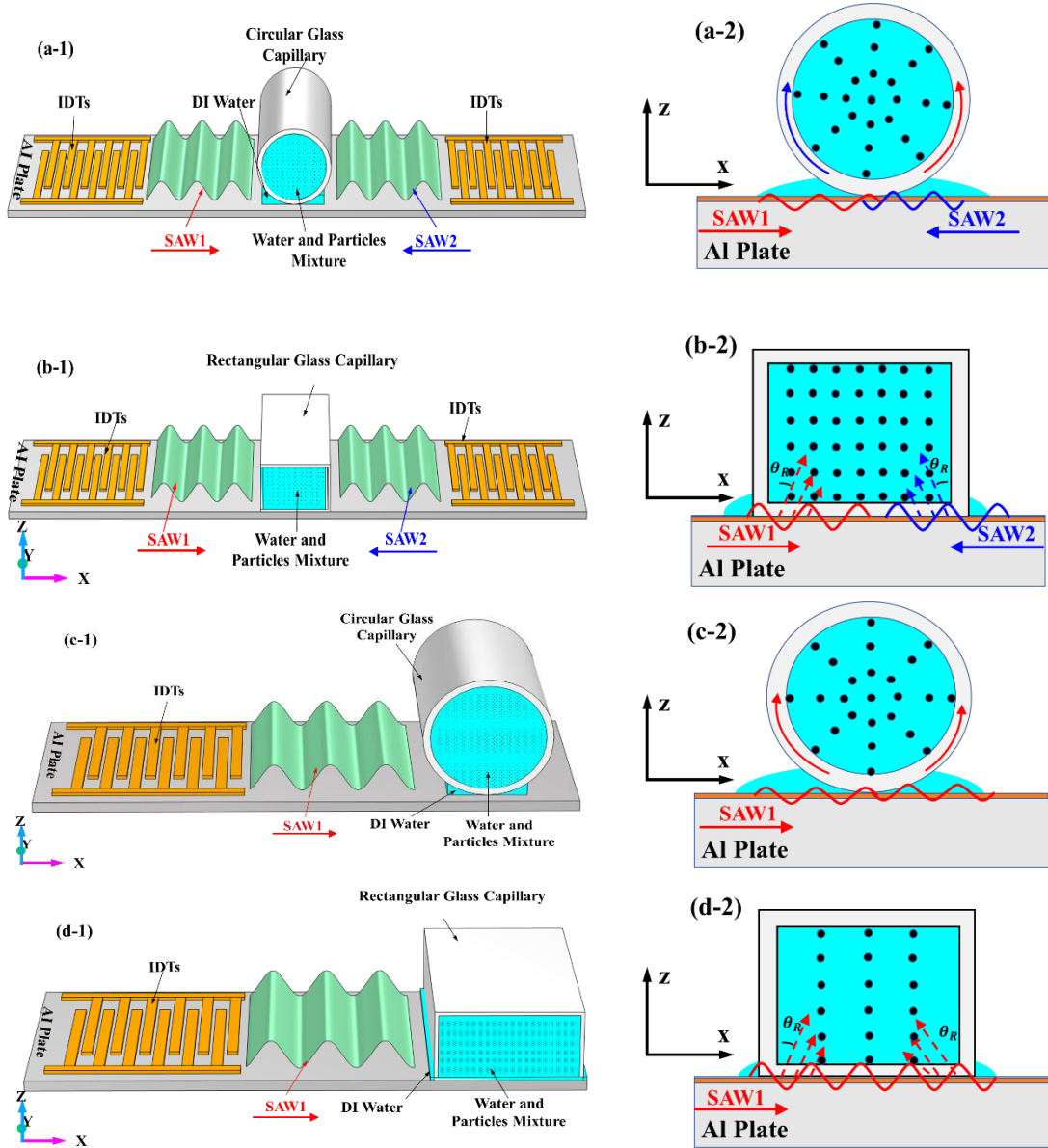


**Fig. 1.** Schematic of the acoustofluidic system composed of a SSAW device with (a-1) circular glass capillary and (b-1) rectangular glass capillary, the principle of SSAW acoustophoresis in (a-2) circular cross-section and (b-2) rectangular cross-section. Schematic of the acoustofluidic system composed of a TSAWS device with (c-1) circular glass capillary and (d-1) rectangular glass capillary, the principle of TSAWS acoustophoresis in (c-2) circular cross-section and (d-2) rectangular cross-section.

Whereas for the rectangular glass capillary case (as shown in **Fig. 1** (d-1)), when the TSAWs are generated and propagated along the substrate surface, the waves are radiated from the substrate surface into the rectangular glass capillary through the water layer. Then the TSAWs will be gradually attenuated along the interface between the rectangular glass capillary and the substrate due to the acoustic damping effect. The TSAWs will be also reflected at the other interface between the capillary and air. The

interference between the radiated TSAWs and reflected TSAWs and the generated acoustic field will be produced in the cross-section as shown in **Fig. 1** (d-2). The SAWs will be radiated into the rectangular capillary through both sides of the solid-liquid interface and propagated with an angle  $\theta_R$  relative to the wall in the rectangular glass capillary, as shown in **Fig. 1** (d-2). The acoustic field within the capillary will be created by the radiated TSAWs and reflected TSAWs that propagated in opposite directions. The ARF will push the microparticles in the circular glass capillary, and then the microparticles patterning will be produced. The mechanisms are similar to those of SSAWs in the rectangular capillary [34].

## 2.2. Modeling of wave propagation inside glass capillary

For the TSAWs, the patterns generated in both the circular and rectangular glass capillaries are caused by the acoustic streaming and the ARF as explained in the Introduction [51]. In this study, pressures fields and patterns generated inside both circular and rectangular glass capillaries were investigated using a physical model, and the results were then compared to rectangular tubes and the SSAWs cases.

### 2.2.1 Wave Propagation inside the capillary tubes

The limiting velocity has been widely used to simplify the process of modeling and simulation in a rectangular glass capillary. When the radius of the circular capillary is larger than the acoustic viscous boundary layer, the limiting velocity method [52] can be used to simplify the acoustic field in the circular capillary. The limiting velocity equations on a planar surface that is normal to  $z$ , are given by [53].

$$u_L = -\frac{1}{4\omega} Re \left\{ u_1 \frac{du_1^*}{dx} + v_1 \frac{dv_1^*}{dy} + u_1^* \left[ (2+i) \left( \frac{du_1}{dx} + \frac{dv_1}{dy} + \frac{dw_1}{dz} \right) - (2+3i) \frac{dw_1}{dz} \right] \right\} \quad (1)$$

$$v_L = -\frac{1}{4\omega} Re \left\{ u_1 \frac{dv_1^*}{dx} + v_1 \frac{dv_1^*}{dy} + v_1^* \left[ (2+i) \left( \frac{du_1}{dx} + \frac{dv_1}{dy} + \frac{dw_1}{dz} \right) - (2+3i) \frac{dw_1}{dz} \right] \right\} \quad (2)$$

where  $\omega$  is the angular frequency, and  $Re$  represents the real part of the internal quantity.  $u_1$ ,  $v_1$  and  $w_1$  are components of first-order complex acoustic velocity vectors in the  $x$ ,  $y$  and  $z$  directions. The superscript  $*$  is the complex conjugate. We then used the coordinate transformation to transform the rectangular coordinate system  $(x, y, z)$  into a cylindrical coordinate system  $(r, \theta, x)$ . Then the first order velocities of sound in the tangent and normal directions at any point are obtained as  $u_{1\tau}$  and  $w_{1n}$ .

$$u_{1\tau} = -u_1 \sin \theta + w_1 \cos \theta \quad (3)$$

$$w_{1n} = -u_1 \cos \theta - w_1 \sin \theta \quad (4)$$

The equation of limiting velocity on the boundary of the circular capillary can be expressed as [33]:

$$u_L^\tau = -\frac{1}{4\omega} Re \left\{ u_{1\tau} \frac{du_{1\tau}^*}{d\tau} + u_{1\tau}^* [(2+i) \left( \frac{du_{1\tau}}{d\tau} + \frac{dw_{1n}}{dn} \right) - (2+3i) \frac{dw_{1n}}{dn}] \right\} \quad (5)$$

where  $\tau$  and  $n$  are the tangent vector and normal vector, respectively.

The distribution of limiting velocity on the circular glass capillary boundary can be obtained from Equation (5). In the numerical simulation, the limiting velocity will be used as the slip edge boundary conditions and replace the sticky boundary layer. This method can reduce the requirement of mesh accuracy and simplify the numerical simulation process. The numerical simulation of circular 2D cross-sections of capillary can be obtained from formula (5).

The sound field mechanics model uses the basic equation to analyze the acoustic and streaming fields. According to the perturbation theory, the first-order acoustic response equation can be obtained as follows [54, 55]:

$$\frac{\partial \rho}{\partial t} + \nabla \cdot (\rho \mathbf{u}_1) = 0 \quad (6)$$

$$\rho \left( \frac{\partial \mathbf{u}_1}{\partial t} + \mathbf{u}_1 \cdot \nabla \mathbf{u}_1 \right) = -\nabla p + \mu \nabla^2 \cdot \mathbf{u}_1 + (\mu_b + \frac{1}{3}\mu) \nabla \nabla \cdot \mathbf{u}_1 \quad (7)$$

where  $\rho$ ,  $\mathbf{u}_1$ ,  $p$ ,  $\mu$  and  $\mu_b$  represent fluid density, fluid velocity, pressure, fluid shear viscosity, and fluid bulk viscosity, respectively.  $\rho_0$  is constant density before the presence of any acoustic wave,  $\rho_1$  and  $p_1$  are the first order perturbations in density  $\rho$  and pressure  $p$ , respectively.

To simplify the model, the fluid was assumed to be homogeneous and isotropic, and thus the viscous dissipation between the fluid and the substrate was ignored. According to the Navier-Stokes equation [50] and Newton's Second Law [56], the spherical microparticles motions in the static fluid are subjected to ARF and hydrodynamic viscous force. According to the perturbation theory, the radiation force can be expressed as [51, 55]:

$$\mathbf{F}^{rad} = \pi a^3 f_2^i(\tilde{\rho}, \tilde{\delta}) E_{ac} \mathbf{k} \quad (8)$$

where  $a$  is the radius of the sphere microparticles,  $f_2^i(\tilde{\rho}, \tilde{\delta})$  is the imaginary part of the

corrected dipole scattering coefficient,  $\tilde{\delta} = \frac{\delta}{a}$ ,  $\delta$  is the thickness of the acoustic boundary layer,  $\tilde{\rho} = \frac{\rho_p}{\rho_0}$ ,  $\rho_p$  is the density of microparticles,  $\rho_0$  is the density of the fluid.  $E_{ac} = \frac{1}{2} \kappa_0 p_a^2$  is the acoustic energy density,  $f_2^i(\tilde{\rho}, \tilde{\delta})$  is the imaginary part of the viscosity-dependent dipole scattering coefficient,  $\mathbf{k}$  is the traveling wave vector. In this paper, the SAW was propagated on the device's surface along one direction, microparticles were manipulated in the  $x$ - $y$  plane and  $x$ - $z$  plane, as shown in **Figs. 1** (c-1) and (d-1). The gravity effect on the spherical microparticles was ignored due to their small sizes.

According to concepts of the Huygens-Fresnel principle and the linear superposition of traveling waves [57], the magnitude of the acoustic field at any point inside the capillary is the sum of the spherical wave contributions (including phase information) from the area of a vibrating surface, thus generating the patterns. Due to the periodicity of the TSAWs, the periodic pressure nodes and anti-nodes will be generated in the capillary by the TSAWs. For the circular capillary, the relationship between the adjacent lines distances and the tilting angle can be given by [57],

$$d_\theta = \frac{v_1}{v_s} \lambda_{SAW} (1 - \frac{v_1}{v_s} \cos\theta)^{-1} \quad (9)$$

For the rectangular capillary, the relationship between the adjacent lines distances and the tilting angle can be given by [39, 57],

$$d_\theta = \frac{v_1}{v_s} \lambda_{SAW} \sin(\theta) \csc(\theta - \sin^{-1}(\frac{v_1}{v_s} \sin\theta)) \quad (10)$$

where  $v_1$  and  $v_s$  are the sound velocity in the fluid and the substrate of the SAW device,  $\lambda_{SAW}$  is the wavelength of the SAW device,  $\theta$  is the angle between the circular glass capillary walls and the SAW propagation direction ( $\theta$  is no more than  $90^\circ$ ),  $\csc$  is the cosecant  $\csc(\theta) = 1/\sin(\theta)$ . From Equation (9) we know that the distances between the adjacent lines will be changed periodically. When the tilting angle is smaller than  $75^\circ$ , the distances will increase with the increasing tilting angle.

### 2.2.2 Simulation results of acoustic pressure distribution in capillary

Simulation results of the microparticles pattern agitated using SSAWs within both the circular and rectangular glass capillaries have been presented in our previous paper

[34]. The theory of finite element method (FEM) was used to discrete the governing equations, which were solved by Newton's iterative method. The acoustic wave travels on the surface of the SAW device substrate, transfers energy to the rectangular glass capillary, and is reflected by the capillary walls forming the acoustic field inside the liquid.

The governing equations of the acoustic wave propagation in liquids are derived using the perturbation method with the assumptions of one-dimensional attenuating acoustic waves, spherical particles. The effects of fluid's viscosity and microparticles' compressibility are negligible which leads to the Helmholtz equation [34]:

$$\nabla^2 \varphi(\mathbf{r}) = -\frac{\omega^2}{c_f^2} \varphi(\mathbf{r}) \quad (11)$$

where  $\nabla \varphi = \mathbf{U}_f$ ,  $\mathbf{U}_f$  is the fluid velocity,  $\omega$  is the wave angular frequency and  $c_f$  is the isentropic derivative of pressure equal to wave speed in the fluid,

The acoustic effects are then coupled into the liquid filled capillaries using the acoustic radiation force,  $F_{ARx}$  generated from a one-dimensional TSAW propagating in the  $x$ -direction defined as follows:

$$F_{ARx} = \left( \frac{2\pi^3 P_{ac}^2 V_p^2 \beta_f}{\lambda^4} \right) \left( \frac{9+2(1-\rho_f/\rho_p)^2}{(2+\rho_f/\rho_p)^2} \right) \quad (12)$$

where  $P_{ac}$  is the acoustic pressure amplitude,  $V_p$  is the particle volume,  $\beta_f$  is the fluid compressibility,  $\lambda$  is the wavelength,  $\rho_f$  is the fluid density, and  $\rho_p$  is the particle density.

The boundary condition to represent the propagation of the TSAWs are modelled using the oscillating wall boundary conditions by defining the velocity of the TSAW propagating on the surface of the SAW device as follows [58]:

$$u_{x-wall} = A_y \zeta \omega e^{-\alpha(0.5w-x)} e^{i[-k(0.5w-x)]} \quad (13)$$

$$u_{y-wall} = A_y \omega e^{-\alpha(0.5w-x)} e^{i[-k(0.5w-x)-\pi/2]} \quad (14)$$

where  $u_{x-wall}$  and  $u_{y-wall}$  are the SAW velocities in  $x$ - and  $y$ -directions, respectively,  $A_y$  is the wave's displacement amplitude in  $y$ -direction,  $w$  is the channel width,  $\alpha$  is the wave attenuation coefficient,  $x$  is the longitudinal direction and  $\zeta$  is the

ratio of the displacement amplitudes in  $x$ - and  $y$ -directions.

The boundary conditions on all the other surfaces are defined as impedance boundary conditions as follows:  $Z_{wall} = \rho_{wall}c_{wall}$ , where  $Z_{wall}$  is the wall's impedance,  $\rho_{wall}$  is the wall density and  $c_{wall}$  is the wave's propagation velocity in the wall. Mesh dependency analysis was performed to obtain the optimum number of mesh elements for high accuracy, and reasonable computational time and the computational mesh was generated with  $\sim 250,000$  and  $\sim 150,000$  unstructured tetrahedral elements for the rectangular and circular tubes, respectively.

This paper mainly focused on analyzing the acoustic wave distribution in the glass capillary using the TSAWs. The simulation results are shown in **Fig. 2** and **Fig. 3**. Two types of capillaries were simulated. The first one is the circular capillary. The outer diameter and the inner diameter of the circular glass capillary tube used in experiments are  $550 \mu\text{m}$  and  $400 \mu\text{m}$ , respectively. The length of the circular glass capillary is about  $15 \text{ mm}$ . The second one is a rectangular capillary, with an outer dimension  $2.3 \text{ mm} \times 0.5 \text{ mm}$  (inner dimension is  $2.0 \text{ mm} \times 0.2 \text{ mm}$ ). The working frequency of the IDTs is  $7.19 \text{ MHz}$ .

The simulation results of the acoustic pressure field inside circular glass capillary are shown in **Figs. 2** (a) to (e). They show that a complicated acoustic field is formed when the SAW is transferred from the surface of the substrates to the circular glass capillary and propagates through the cross-section of the circular capillary. When the circular capillary tube is placed parallel to the IDTs (**Fig. 2** (a-1)), the pressure node lines are formed parallel to the IDTs fingers and capillary tube wall. This will result in the particles accumulated on these pressure node lines, thus forming linear patterns parallel to the IDTs and capillary tube wall. Placing the circular capillary tube with a  $15^\circ$  tilting angle with respect to the IDTs (**Fig. 2** (b-1)), results in the formation of the checkerboard acoustic pressure field with pressure node lines both parallel and perpendicular to the IDT fingers and capillary tube walls. This causes the particles to form linear patterns parallel to the IDT, but the lines become slightly jagged. When the tilting angle is increased to  $30^\circ$  (**Fig. 2** (c-1)), the acoustic pressure field in the circular glass tube becomes somewhat distorted, which results in the distortion of the particle patterns and

no linearity can be observed, which is similar to the patterns generated using the SSAWs [34]. Further increasing the tilting angle to  $45^\circ$  (**Fig. 2 (d-1)**) and  $60^\circ$  (**Fig. 2 (e-1)**) causes the acoustic pressure field to become distorted, and the microparticles do not form any clear line patterns in the capillary tube.

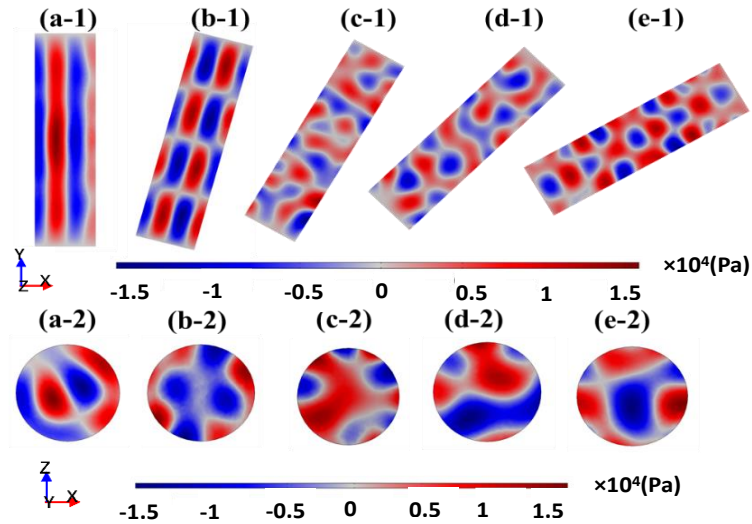


**Fig. 2.** Acoustic pressure field in the circular glass capillary with different tilting angle (a) parallel, (b)  $15^\circ$ , (c)  $30^\circ$ , (d)  $45^\circ$ , (e)  $60^\circ$ . (1) is the top view and (2) is the cross-sectional view.

**Figs. 3 (a) to (e)** present the simulation results of the acoustic pressure field inside the rectangular glass capillary using the COMSOL Multiphysics (5.6) [34]. When the rectangular glass capillary is placed parallel to the IDT (**Fig. 3 (a)**), the acoustic pressure field forms clear linear pressure node patterns parallel to the capillary walls as well as the IDTs. The particles will be accumulated on these pressure node lines and patterned into lines parallel to the IDTs. Increasing the angle between the rectangular capillary tube to  $15^\circ$  (**Fig. 3 (b)**) results in a slight distortion in the acoustic pressure and the pressure node lines. This causes the particle pattern lines to become slightly distorted as well. Further increase in the tilting angle to  $30^\circ$  (**Fig. 3 (c)**),  $45^\circ$  (**Fig. 3 (d)**), and  $60^\circ$  (**Fig. 3 (e)**) causes the acoustic pressure field to form checker-board patterns, and thus the particle patterns will become more and more distorted without formation of any clear linear patterns. The simulation results show good agreements with the experimental data (see in **Figs. 4 and 5**).

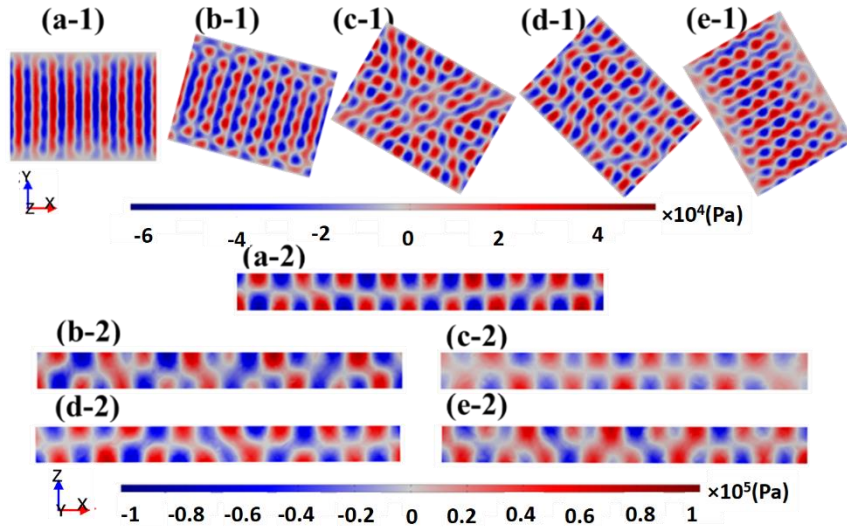


**Fig. 3.** Acoustic pressure field in rectangular glass capillary with different tilting angle (a) parallel, (b) 15°, (c) 30°, (d) 45°, (e) 60°. (1) is the top view and (2) is the cross-sectional view.

### 3. Results and discussion

#### 3.1 Microparticle patterning in glass capillary: tilting angle effects

To verify the effects of the tilting angle, the SAW device with a frequency of 6.05 MHz was used to produce the patterns generated in the circular glass capillary with 550  $\mu\text{m}$  outer diameter and 400  $\mu\text{m}$  inner diameter. The comparison between the SSAW and the TSAW is illustrated in the supporting information **Fig. S2**. **Fig. 4** shows the captured images of patterns at different tilting angles in the middle of the circular glass capillary. The light green lines in **Fig. 4** are the positions of boundaries inside the glass capillary. Results clearly show that when the tilting angle is  $0^\circ$ , the patterning is clear and the straight lines in the patterns are parallel to the wall of the circular glass capillary. With the increasing tilting angle, the quality of straight lines becomes worse. When the tilting angle reaches  $45^\circ$ , the lines perpendicular to the capillary walls appear, but the lines parallel to the capillary walls become unclear. When the tilting angle is larger than  $45^\circ$ , the patterned lines are disappeared, and the patterns are irregular. We can observe the patterning of microparticles along the wall of the circular glass capillary.

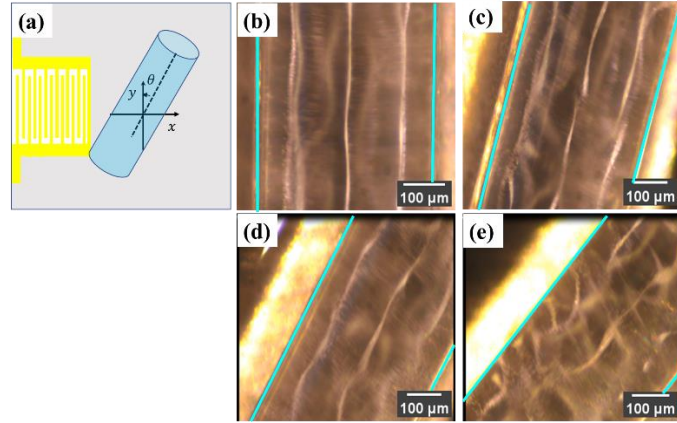


**Fig. 4.** The patterning in the circular glass capillary with different tilting angles. (a)  $\theta=0^\circ$ , (b)  $\theta=15^\circ$ , (c)  $\theta=30^\circ$ , (d)  $\theta=45^\circ$ . The resonance frequency of IDTs is 6.05 MHz, and the outer diameter of the circular glass capillary is 550  $\mu\text{m}$ . The green line is inner boundary position of the glass capillary.

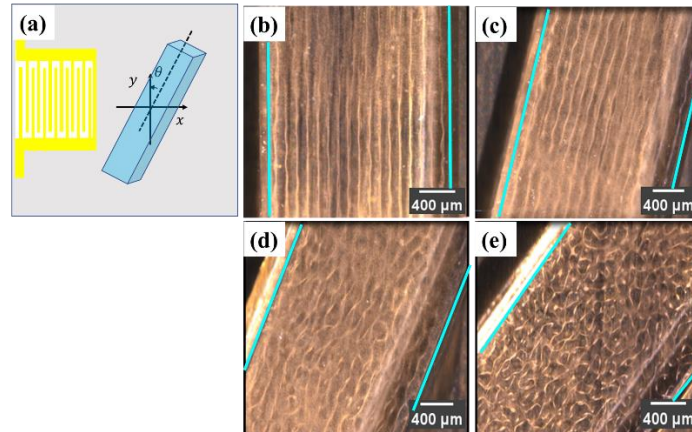


**Fig. 5.** The patterns in the rectangular glass capillary (width 2.3 mm and height 0.5 mm) with different tilting angles. (a) the schematic top view of a rectangular glass capillary located at a tilting angle, (b)  $\theta=0^\circ$ , (c)  $\theta=15^\circ$ , (d)  $\theta=30^\circ$ , (e)  $\theta=45^\circ$ . The frequency is 6.05 MHz. The green line is inner boundary position of the glass capillary.

**Fig. 5 (a)** shows a schematic top view of a rectangular glass capillary located at a tilting angle in the middle of the circular glass capillary,  $\theta$ , on the thin film-based SAW device. In these experiments, the resonant frequency applied to the IDTs was 6.05 MHz, and the outer dimension of the rectangular capillary is 2.3 mm  $\times$  0.5 mm (inner dimension is 2.0mm  $\times$  0.2 mm). When the tilting angle was  $\theta=0^\circ$ , the rectangular glass capillary was positioned parallel to IDTs. **Fig. 5 (b)** shows patterns generated in the rectangular glass capillary, in which the lines are parallel to the capillary wall. When the tilting angle is changed to  $\theta=15^\circ$ , the pattern lines are similar to those at  $\theta=0^\circ$  (**Fig. 5 (c)**). When the tilting angle is about  $\theta=30^\circ$ , the pattern lines are not straight, and the regularly distributed waves patterns (which have been commonly believed due to Lamb

waves [1]) appear as shown in **Fig. 5** (d). When the tilting angle is further increased above  $\theta=45^\circ$ , no clear patterned lines are observed as shown in **Fig. 5** (e). These observations are consistent with SSAW generated alignment patterns reported in our previous paper [34].

The adjacent line distances were estimated based on the geometry of the tubes and the open-source image processing software “ImageJ”. With the tilting angle increased from  $\theta=0^\circ$  to  $\theta=45^\circ$ , adjacent lines distance in the circular glass capillary (with 550  $\mu\text{m}$  outer diameter in **Fig. 4**) becomes increased from 88  $\mu\text{m}$  to 113  $\mu\text{m}$ . When the tilting angle is increased from  $\theta=0^\circ$  to  $\theta=30^\circ$ , the distance of the adjacent line in the rectangular glass capillary (width 2.3 mm and height 0.5 mm in **Fig. 5**) is increased from 113  $\mu\text{m}$  to 167  $\mu\text{m}$ . The estimated adjacent distances of lines as a function of the tilting angle are shown in **Fig. 6**. According to the Equations (9) and (10), there is a linear relationship between the adjacent lines distance and the tilting angle when the tilting angle is smaller than  $45^\circ$ . The estimated distance between the adjacent lines is increased with the tilting angle. The experimental results can be verified using the predictive Equation (9), as shown in **Fig. 6**. There is a deviation between the experimental results and the simulation results, which is induced by the wavelength deviation and the tilting angle deviation used in simulation and experiment.

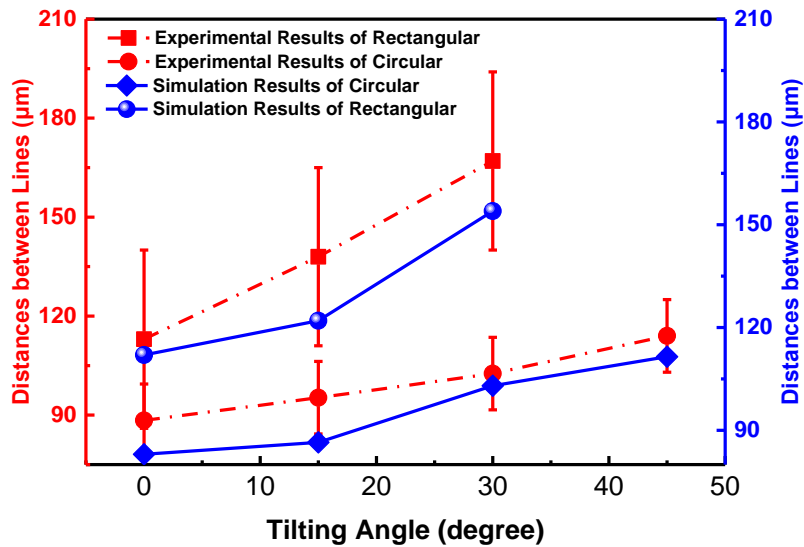


**Fig. 6.** The relationship between the adjacent lines distance and tilting angle.

### 3.2 Frequency effects

**Fig. 7** shows the influences of the resonance frequency of SAW devices on the

patterns generated inside the circular capillary, in which three different resonance frequencies were applied, i.e., 6.05, 13.15, and 27.37 MHz, respectively. The outer diameter of the circular glass tube was 550  $\mu\text{m}$ , and the inside diameter was 400  $\mu\text{m}$ . The light green lines in **Fig. 7** are the positions of boundaries inside the glass capillary. Results clearly show that with the increase of the frequency, the number of the pattern lines is increased, and the distance between the adjacent lines is decreased, as shown in **Fig. 7** (d). When the diameter of the circular glass capillary is increased to 1 mm, the number of the pattern lines in the capillary from top-view is increased from 3 to 6, as shown in **Fig. 7** (a) and **Fig. 10** (b). With increasing frequency, the particle patterning becomes less clear, and lines are changed from continuously straight to intermittent. This may be caused by the complicated acoustic wave field generated inside the circular glass capillary. The distance of the adjacent particle lines is decreased with the increase of the SAW device's frequency. **Fig. 7** (d) shows the obtained average distances between adjacent lines at different frequencies, and they are about half of the wavelengths, indicating that they are caused by the SAWs, not due to the resonance of liquid within the glass capillaries. Results also show that the generated acoustic wave and microparticle distribution patterns are related to the frequency of the IDTs, but not related to the radius of the capillary and acoustic wave powers. The red area is the standard deviation area. The maximum error occurs at 13.15 MHz, and the minimum error occurs at 27.37 MHz. This is because that the patterns formed at 13.15 MHz is not uniformly distributed. The distance between the adjacent lines at 27.37 MHz is much narrower than those at other frequencies. The patterning in the circular glass capillary with different tilting angle under 27.37 MHz is illustrated in the supporting information **Fig. S3**.

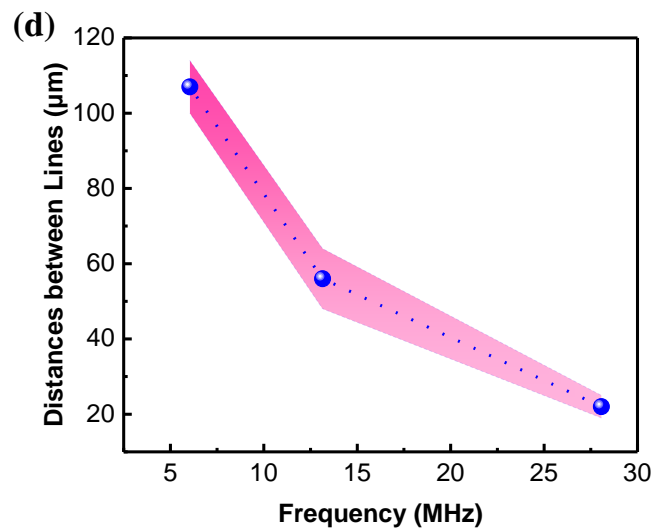
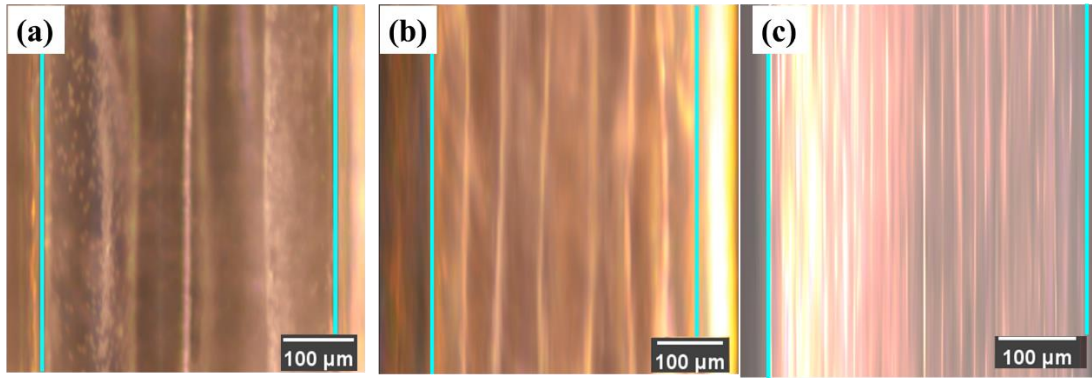


**Fig. 7.** The patterning in the circular glass capillary with different frequencies: (a) 6.05 MHz, (b) 13.15 MHz, and (c) 27.37 MHz, respectively. The outer diameter of the circular glass tube was 550  $\mu\text{m}$ , and the inside diameter was 400  $\mu\text{m}$ . (d) the distances between the adjacent lines at different frequencies. The green line is inner boundary position of the glass capillary and the red area represents the standard deviation.

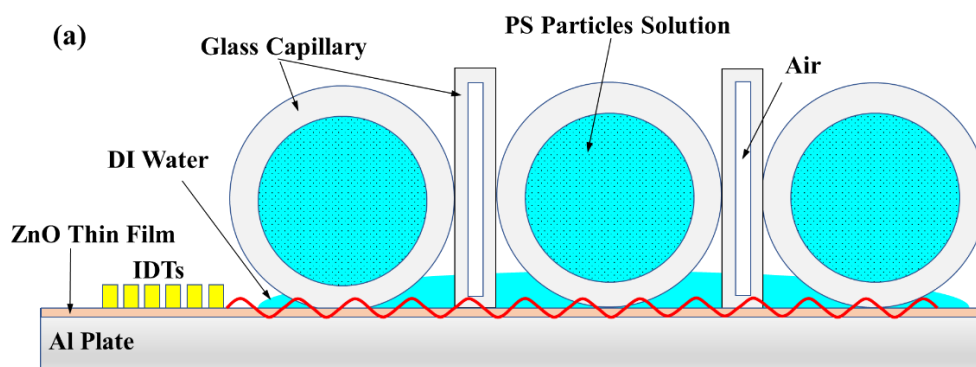
## 4. Demonstration of acoustofluidics manipulation applications

### 4.1. Capillary patterning with multiplexing Technique

**Fig. 8** (a) shows the schematic of the experimental setup. Two-capillary and three-capillary multiplexing (**Figs. 8** (d) and (e)) have been performed. In our experiments, the resonance frequency of IDTs was 6.05 MHz. The inside and outside diameters of the circular glass capillary were 400  $\mu\text{m}$  and 550  $\mu\text{m}$ , respectively. To prevent interference from the adjacent capillary, the circular capillary tubes were separated by a rectangular glass capillary with 100  $\mu\text{m}$  width without any water inside. **Figs. 8** (b) and (c) show the steady state distribution of the PS microparticles in the two- and three-circular glass capillaries multiplexing without applying any SAWs, and the

microparticles are randomly distributed. **Figs. 8** (d) and (e) show the patterns generated in the circular glass capillary after the SAWs were switched on for 20 milliseconds when the output power (i.e., forward power) of amplifier is 200 mW, which was measured by an RF power meter (Racal Instruments 9104). The results show regular and stable patterns in the circular glass capillaries for both cases with two or three capillaries. This indicates that along the wave propagating paths, multiple glass capillaries can be placed in batch patterning work. These results are caused by the interference between the SAW wavefront and the capillary walls. Part of TSAWs will be coupled into an overlaying fluid at all points along the channel height, and the other part will propagate along the substrate. The interference between the fluid wavefronts and the SAW wavefronts occurs, and the generated patterns will be produced in the capillary along the path of TSAWs.

With a wide range of acoustic frequencies, this array of two or three capillaries can selectively manipulate different size particles or generate higher throughput of several analytes. It is also a potential technology that can be used as a high-throughput microfluidics flow cytometry. The mechanical properties of tens to hundreds of individual cells can be measured through the network of circular glass capillaries. This technology has a remarkable potential for implementation in both biological laboratories and clinical settings [59].



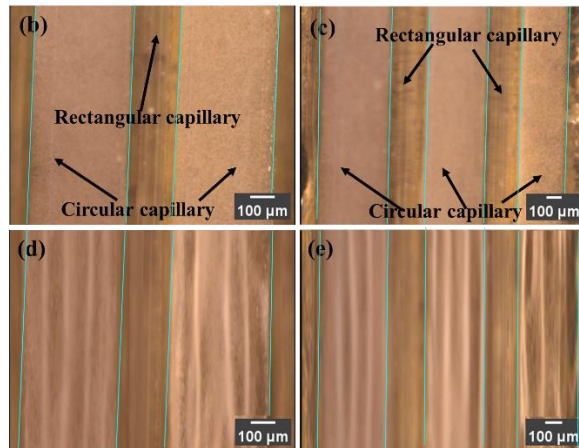


**Fig. 8.** The schematic of the experimental setup with multiplexing technique. The patterning in the circular glass capillary when (b) and (c) SAW is off, (d) SAW is on with two capillaries, (e) SAW is on with three capillaries (the resonance frequency of IDTs is 6.05 MHz). The green line is inner boundary position of the glass capillary.

#### 4.2. Formation of solidified particle-hydrogel patterns in glass capillaries

To form a solid gel pattern of the microparticle patterns in the circular glass capillary, the PS/DI water/agarose (fisher bioreagents BP1356-500) mixture was used to immobilize the PS particles. In this experiment, the resonant frequency of the SAW device was 6.04 MHz. **Fig. 9** shows the distributions of the microparticles before and after agitation using the SAWs. The light is illuminated from different directions in our experiments. In **Figs. 9** (a) and (b), the light is illuminated from the above-left and above-right of capillary, and the particle patterns are appeared bright. In **Figs. 9** (c) and (d), the light is illuminated from under the capillary, so the particles appear dark. When the SAW is activated, the microparticles (randomly distributed in **Fig. 9** (a)) are observed to move quickly to nodes positions forming line particle patterns along the length direction. The top view of the patterning in the circular glass capillary is shown in **Fig. 9** (b). It shows that the microparticles are concentrated and patterned into lines along the capillary under the agitation of TSAWs. After about 10 min, the particle patterns were fixed in the capillary. The microparticles inside the capillary were observed using an optical microscope (Nikon ECLIPSE LV100). After a few hours, the enlarged images of well-formed aligned microparticle patterns inside the capillary tube are shown in **Figs. 9** (c) and (d). The PS microparticles were observed to be aligned rapidly as soon as the signal was applied. With the SAWs power increase, the alignment

patterns do not change significantly, but the time to form the patterning in the circular glass capillary is shortened. This study demonstrated that this method could restrict the cells or proteins to a fixed location and realize the bio-patterning. It is possible to individually examine the changes in cells or proteins during their growth process. [60].

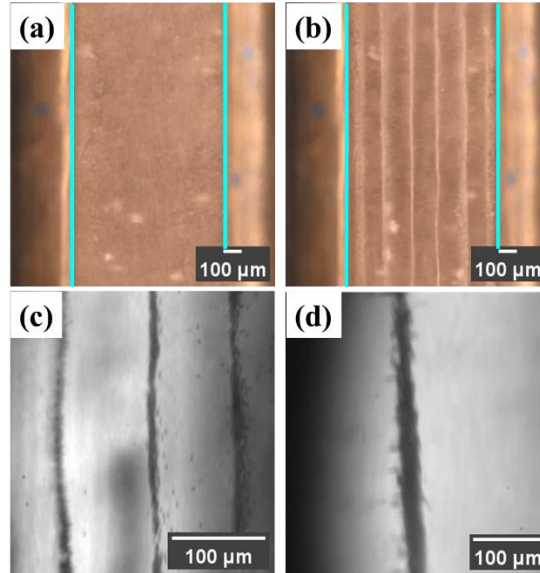


**Fig. 9.** The patterns in circular glass capillary (OD=1.0mm, ID=800  $\mu\text{m}$ ) with a single IDT. (a) the microparticles suspended in PS/DI water/agarose mixture with SAW off (the light is illuminated from the above-left and the above-right). (b) the pattern of the microparticles in PS/DI water/agarose mixture with SAW on (the resonance frequency of IDT is 6.04 MHz, and the light is illuminated from the above-left and the above-right). (c) the micrograph of microparticles pattern in PS/DI water/agarose mixture under microscope with 20 times magnification (the light is irradiated from below the capillary). (d) the micrograph of microparticles pattern in PS/DI water/agarose mixture under microscope with 50 times magnification (the light is irradiated from below the capillary). The green line is inner boundary position of the glass capillary.

### 4.3. Flexible bending demonstration

ZnO/Al foil-based flexible SAW device (The thicknesses of ZnO and Al foil are 5  $\mu\text{m}$  and 50  $\mu\text{m}$ , respectively) was applied to wrap around circular glass capillary. **Fig. 10 (a)** shows that the flexible SAW device was bent and wrapped around the circular glass tubes to manipulate the particles or cells inside the tubes. The circular glass capillary (outer diameter is 550  $\mu\text{m}$  and inner diameter was 400  $\mu\text{m}$ ) was put onto the wrapped SAW device, and a droplet of DI water was dropped onto the surface between the circular glass capillary and the SAW device to increase the wave transfer from the substrate into the glass tube. The bending angle of the SAW devices was changed from 0° to 45°, and the obtained particle patterns in capillary are shown in **Figs. 10 (b)-(d)**.

These results show that the microparticles are patterned into regularly distributed lines and the lines are parallel to the wall of the circular glass capillary, although the distances between the adjacent patterned lines are a bit varied. These results show that the TSAWs technology has potential applications in flexible and wearable applications including surface conforming devices, soft robotics, flexible sensors, and electronics [61].

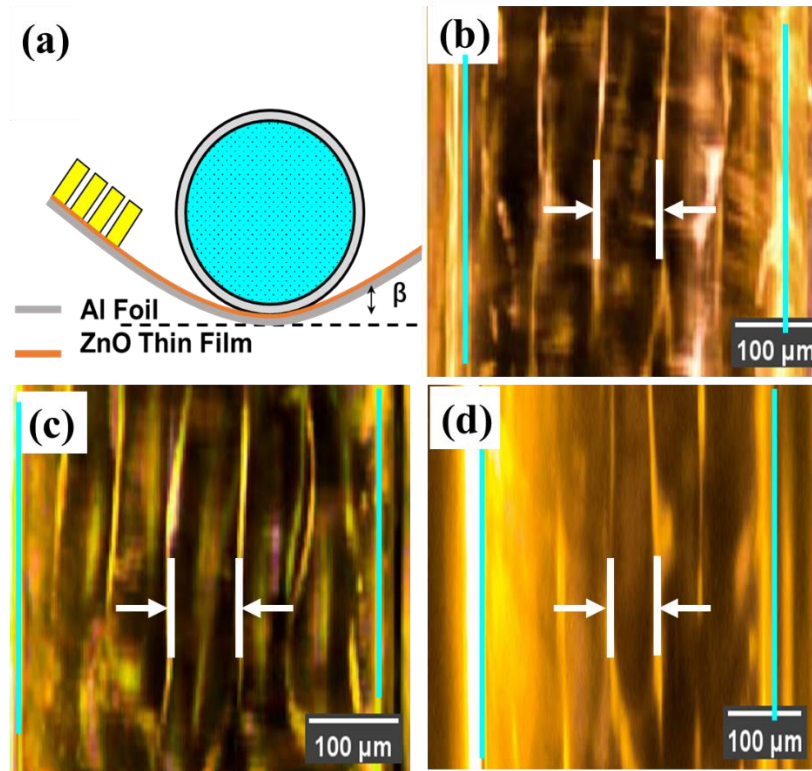


**Fig. 10.** (a) The schematic of the experimental setup used for thin film SAW device experiments. The outer diameter of the capillary is  $550\ \mu\text{m}$  and inner diameter is  $400\ \mu\text{m}$ , and the resonance frequency of IDTs is  $13.15\ \text{MHz}$ . The patterning in the circular glass capillary when the bending angle is (b)  $\beta=0^\circ$ , (c)  $\beta=30^\circ$  and (d)  $\beta=45^\circ$ . The green line is inner boundary position of the glass capillary.

## 5 Conclusions

In this paper, propagating SAWs were applied to generate microparticle patterning in both circular and rectangular glass capillaries. Numerical analysis revealed the acoustic pressure field distribution inside the circular and rectangular glass capillaries. The relationships among the pattern generation and the SAWs frequency, the circular glass capillary diameter, and the tilting angles were investigated. The experimental results showed that the travelling waves patterned the microparticles along lines parallel to the wall of the circular glass capillary, and a clear pattern was observed when the

tilting angle was below 45°. Results also showed that the distance between two adjacent linear patterns is dependent only on the frequency of the SAWs wavelength and is not related to the diameter of the capillary. Compared to the SSAWs, the TSAWs device can generate the acoustic field using one IDT. We explored their potential applications in different scenarios, including multiple capillary patterning, solidified particle-hydrogel patterns, and flexible bending demonstration, which can still pattern, concentrate, and focus the microparticles or biological cells, even under a large bending state. The experimental results demonstrated the possibility of manipulating the particles in the glass capillary using the travelling SAWs.

### **Acknowledgement**

This work was supported by the National Natural Science Foundation of China (NSFC 11404054, 61601104), the Engineering Physics and Science Research Council of UK (EPSRC EP/P018998/1) and International Exchange Grant (IEC/NSFC/201078) through Royal Society UK and the NSFC, the Natural Science Foundation of Hebei Province (F2019501025, F2020501040), and the Fundamental Research Funds for the Central Universities (2023FZD002).

### **References**

- [1] Y.Q. Fu, J. Luo, N.-T. Nguyen, A. Walton, A.J. Flewitt, X.-T. Zu, Y. Li, G. McHale, A. Matthews, E. Iborra, *Advances in piezoelectric thin films for acoustic biosensors, acoustofluidics and lab-on-chip applications*, *Progress in Materials Science*, 89 (2017) 31-91.
- [2] A. Ozcelik, J. Rufo, F. Guo, Y. Gu, P. Li, J. Lata, T.J. Huang, *Acoustic tweezers for the life sciences*, *Nature methods*, 15 (2018) 1021-1028.
- [3] D. Jiang, J. Liu, Y. Pan, L. Zhuang, P. Wang, T. Research, *Surface acoustic wave (SAW) techniques in tissue engineering*, *Cell*, 386 (2021) 215-226.
- [4] X. Ding, P. Li, S.-C.S. Lin, Z.S. Stratton, N. Nama, F. Guo, D. Slotcavage, X. Mao, J. Shi, F. Costanzo, *Surface acoustic wave microfluidics, Lab on a Chip*, 13 (2013) 3626-3649.
- [5] D. Mandal, S. Banerjee, *Surface acoustic wave (SAW) sensors: Physics, materials, and applications*, *Sensors*, 22 (2022) 820.
- [6] M.B. Mazalan, A.M. Noor, Y. Wahab, S. Yahud, W.S.W.K. Zaman, *Current Development in Interdigital Transducer (IDT) Surface Acoustic Wave Devices for Live Cell In Vitro Studies: A Review*, *Micromachines*, 13 (2021) 30.
- [7] M. Stringer, Z. Zeng, X. Zhang, Y. Chai, W. Li, J. Zhang, H. Ong, D. Liang, J. Dong, Y. Li, Y. Fu, X. Yang, *Methodologies, technologies, and strategies for acoustic streaming-based acoustofluidics*, *Applied*

Physics Reviews, 10 (2023) 011315.

- [8] A. Guex, N. Di Marzio, D. Eglin, M. Alini, T. Serra, The waves that make the pattern: A review on acoustic manipulation in biomedical research, *Materials Today Bio*, 10 (2021) 100110.
- [9] M. Agostini, M. Cecchini, Ultra-high-frequency (UHF) surface-acoustic-wave (SAW) microfluidics and biosensors, *Nanotechnology*, 32 (2021) 312001.
- [10] X. Liu, T. Zheng, C. Wang, Three-dimensional modeling and experimentation of microfluidic devices driven by surface acoustic wave, *Ultrasonics*, 129 (2023) 106914.
- [11] J. Wang, F. Cai, Q. Lin, D. Zhao, H. Zheng, Acoustic radiation force dependence on properties of elastic spherical shells in standing waves, *Ultrasonics*, 127 (2023) 106836.
- [12] H.N. Açıkgöz, A. Karaman, M.A. Şahin, Ö.R. Çaylan, G.C. Büke, E. Yıldırım, İ.C. Eroğlu, A.E. Erson-Bensan, B. Çetin, M.B. Özer, Assessment of silicon, glass, FR4, PDMS and PMMA as a chip material for acoustic particle/cell manipulation in microfluidics, *Ultrasonics*, 129 (2023) 106911.
- [13] K. Wang, W. Zhou, Z. Lin, F. Cai, F. Li, J. Wu, L. Meng, L. Niu, H. Zheng, Sorting of tumour cells in a microfluidic device by multi-stage surface acoustic waves, *Sensors and Actuators B: Chemical*, 258 (2018) 1174-1183.
- [14] C. Mu, Z. Zhang, M. Lin, Z. Dai, X. Cao, Development of a highly effective multi-stage surface acoustic wave SU-8 microfluidic concentrator, *Sensors and Actuators B: Chemical*, 215 (2015) 77-85.
- [15] M. Wu, A. Ozcelik, J. Rufo, Z. Wang, R. Fang, T. Jun Huang, Acoustofluidic separation of cells and particles, *Microsystems & Nanoengineering*, 5 (2019) 1-18.
- [16] M. Wu, K. Chen, S. Yang, Z. Wang, P.-H. Huang, J. Mai, Z.-Y. Li, T.J. Huang, High-throughput cell focusing and separation via acoustofluidic tweezers, *Lab on a Chip*, 18 (2018) 3003-3010.
- [17] M. Wu, P.H. Huang, R. Zhang, Z. Mao, C. Chen, G. Kemeny, P. Li, A.V. Lee, R. Gyanchandani, A.J. Armstrong, Circulating Tumor Cell Phenotyping via High - Throughput Acoustic Separation, *Small*, 14 (2018) 1801131.
- [18] K. Chen, N. Wang, M. Guo, X. Zhao, H. Qi, C. Li, G. Zhang, L. Xu, Detection of SF6 gas decomposition component H2S based on fiber-optic photoacoustic sensing, *Sensors and Actuators B: Chemical*, 378 (2023) 133174.
- [19] M.L.S. Silva, Microfluidic devices for glycobiomarker detection in cancer, *Clin. Chim. Acta*, 521 (2021) 229-243.
- [20] F. Wu, M.H. Shen, J. Yang, H. Wang, R. Mikhaylov, A. Clayton, X. Qin, C. Sun, Z. Xie, M. Cai, An enhanced tilted-angle acoustofluidic chip for cancer cell manipulation, *IEEE Electron Device Letters*, 42 (2021) 577-580.
- [21] W. Zhou, J. Le, Y. Chen, Y. Cai, Z. Hong, Y. Chai, Recent advances in microfluidic devices for bacteria and fungus research, *TrAC Trends in Analytical Chemistry*, 112 (2019) 175-195.
- [22] K. Mutafulopulos, P. Spink, C. Lofstrom, P. Lu, H. Lu, J. Sharpe, T. Franke, D. Weitz, Traveling surface acoustic wave (TSAW) microfluidic fluorescence activated cell sorter ( $\mu$ FACS), *Lab on a Chip*, 19 (2019) 2435-2443.
- [23] F. Pian, Q. Wang, M. Wang, P. Shan, Z. Li, Z. Ma, A shallow convolutional neural network with elastic nets for blood glucose quantitative analysis using Raman spectroscopy, *Spectrochimica Acta Part A: Molecular and Biomolecular Spectroscopy*, 264 (2022) 120229.
- [24] Q. Wang, F. Pian, M. Wang, S. Song, Z. Li, P. Shan, Z. Ma, Quantitative analysis of Raman spectra for glucose concentration in human blood using Gramian angular field and convolutional neural network, *Spectrochimica Acta Part A: Molecular and Biomolecular Spectroscopy*, 275 (2022) 121189.
- [25] Q. Wang, S. Song, L. Li, D. Wen, P. Shan, Z. Li, Y. Fu, An extreme learning machine optimized by

differential evolution and artificial bee colony for predicting the concentration of whole blood with Fourier Transform Raman spectroscopy, *Spectrochimica Acta Part A: Molecular and Biomolecular Spectroscopy*, 292 (2023) 122423.

[26] C. Devendran, K. Choi, J. Han, Y. Ai, A. Neild, D. Collins, Diffraction-based acoustic manipulation in microchannels enables continuous particle and bacteria focusing, *Lab on a Chip*, 20 (2020) 2674-2688.

[27] Y. Gu, C. Chen, J. Rufo, C. Shen, Z. Wang, P.-H. Huang, H. Fu, P. Zhang, S.A. Cummer, Z. Tian, T.J. Huang, Acoustofluidic Holography for Micro- to Nanoscale Particle Manipulation, *ACS Nano*, 14 (2020) 14635-14645.

[28] A. Fakhouri, C. Devendran, A. Ahmed, J. Soria, A. Neild, The size dependant behaviour of particles driven by a travelling surface acoustic wave (TSAW), *Lab on a Chip*, 18 (2018) 3926-3938.

[29] S. Sachs, M. Baloochi, C. Cierpka, J. König, On the acoustically induced fluid flow in particle separation systems employing standing surface acoustic waves—Part I, *Lab on a Chip*, 22 (2022) 2011-2027.

[30] N. Zhang, A. Horesh, J. Friend, Manipulation and Mixing of 200 Femtoliter Droplets in Nanofluidic Channels Using MHz - Order Surface Acoustic Waves, *Advanced Science*, 8 (2021) 2100408.

[31] Y. Gu, C. Chen, Z. Mao, H. Bachman, R. Becker, J. Rufo, Z. Wang, P. Zhang, J. Mai, S. Yang, Acoustofluidic centrifuge for nanoparticle enrichment and separation, *Science advances*, 7 (2021) eabc0467.

[32] Z. Wang, J. Rich, N. Hao, Y. Gu, C. Chen, S. Yang, P. Zhang, T.J. Huang, Acoustofluidics for simultaneous nanoparticle-based drug loading and exosome encapsulation, *Microsystems & Nanoengineering*, 8 (2022) 1-11.

[33] G. Liu, J. Lei, F. Cheng, K. Li, X. Ji, Z. Huang, Z. Guo, Ultrasonic particle manipulation in glass capillaries: a concise review, *Micromachines*, 12 (2021) 876.

[34] S. Maramizonouz, C. Jia, M. Rahmati, T. Zheng, Q. Liu, H. Torun, Q. Wu, Y. Fu, Acoustofluidic Patterning inside Capillary Tubes Using Standing Surface Acoustic Waves, *International Journal of Mechanical Sciences*, 214 (2022) 106893.

[35] J.P. Lata, F. Guo, J. Guo, P.H. Huang, J. Yang, T.J. Huang, Surface acoustic waves grant superior spatial control of cells embedded in hydrogel fibers, *Advanced Materials*, 28 (2016) 8632-8638.

[36] Jian Zhou, Yihao Guo, Yong Wang, Zhangbin Ji, Qian Zhang, Fenglin Zhuo, Jingting Luo, Ran Tao, Jin Xie, Julien Reboud, Glen McHale, Shurong Dong, Jikui Luo, Huigao Duan, Yongqing Fu, Flexible and Wearable Acoustic Wave Technologies, *Appl. Phys. Rev.*, 10 (2023) 021311.

[37] T. Peng, M. Zhou, S. Yuan, C. Fan, B. Jiang, Numerical investigation of particle deflection in tilted-angle standing surface acoustic wave microfluidic devices, *Applied Mathematical Modelling*, 101 (2022) 517-532.

[38] S. Maramizonouz, X. Tao, M. Rahmati, C. Jia, R. Tao, H. Torun, T. Zheng, H. Jin, S. Dong, J. Luo, Flexible and bendable acoustofluidics for particle and cell patterning, *International Journal of Mechanical Sciences*, 202 (2021) 106536.

[39] M. Xu, P.V. Lee, D. Collins, Microfluidic acoustic sawtooth metasurfaces for patterning and separation using traveling surface acoustic waves, *Lab on a Chip*, 22 (2022) 90-99.

[40] D.J. Collins, A. Neild, Y. Ai, Highly focused high-frequency travelling surface acoustic waves (SAW) for rapid single-particle sorting, *Lab on a Chip*, 16 (2016) 471-479.

[41] Z. Ma, D.J. Collins, Y. Ai, Single-actuator bandpass microparticle filtration via traveling surface acoustic waves, *Colloid Interface Science Communications*, 16 (2017) 6-9.

[42] R. Derakhshan, A. Mahboubidoust, A. Ramiar, Design of a novel optimized microfluidic channel for

CTCs separation utilizing a combination of TSAWs and DEP methods, *Chemical Engineering Processing-Process Intensification*, 167 (2021) 108544.

[43] G. Liu, Z. Li, X. Li, Y. Li, H. Tang, M. Wang, Z. Yang, Design and experiment of a focused acoustic sorting chip based on TSAW separation mechanism, *Microsystem Technologies*, 26 (2020) 2817-2828.

[44] G. Liu, M. Wang, X. Li, Y. Li, P. Li, Z. Li, X. Ma, Separation of particles using the focused acoustic sorting chip based on the wettability treatment, *AIP Advances*, 11 (2021) 035320.

[45] Z. Mao, P. Li, M. Wu, H. Bachman, N. Mesyngier, X. Guo, S. Liu, F. Costanzo, T.J. Huang, Enriching nanoparticles via acoustofluidics, *Acs Nano*, 11 (2017) 603-612.

[46] G. Destgeer, K.H. Lee, J.H. Jung, A. Alazzam, H.J. Sung, Continuous separation of particles in a PDMS microfluidic channel via travelling surface acoustic waves (TSAW), *Lab on a Chip*, 13 (2013) 4210-4216.

[47] Z. Ma, D.J. Collins, J. Guo, Y. Ai, Mechanical properties based particle separation via traveling surface acoustic wave, *Anal. Chem.*, 88 (2016) 11844-11851.

[48] M. Tayebi, R. O'Rorke, H.C. Wong, H.Y. Low, J. Han, D.J. Collins, Y. Ai, Massively multiplexed submicron particle patterning in acoustically driven oscillating nanocavities, *Small*, 16 (2020) 2000462.

[49] M. Settnes, H. Bruus, Forces acting on a small particle in an acoustical field in a viscous fluid, *Physical Review E*, 85 (2012) 016327.

[50] M. Kumar, D.L. Feke, J.M. Belovich, Fractionation of cell mixtures using acoustic and laminar flow fields, *Biotechnol. Bioeng.*, 89 (2005) 129-137.

[51] Y. Fan, X. Wang, J. Ren, F. Lin, J.J.M. Wu, Recent advances in acoustofluidic separation technology in biology, *Microsystems & Nanoengineering*, 8 (2022) 1-16.

[52] J. Lei, F. Cheng, G. Liu, K. Li, Z. Guo, Dexterous formation of unconventional Chladni patterns using standing bulk acoustic waves, *Applied Physics Letters*, 117 (2020) 184101.

[53] J. Lei, P. Glynne-Jones, M. Hill, Acoustic streaming in the transducer plane in ultrasonic particle manipulation devices, *Lab on a Chip*, 13 (2013) 2133-2143.

[54] V.R. Faradonbeh, S. Rabiei, H. Rabiei, M. Goodarzi, M.R. Safaei, C. Lin, Power-law fluid micromixing enhancement using surface acoustic waves, *Journal of Molecular Liquids*, 347 (2022) 117978.

[55] M. Settnes, H. Bruus, Forces acting on a small particle in an acoustical field in a viscous fluid, *Physical Review E*, 85 (2012) 016327.

[56] A.D. Pierce, *Acoustics: an introduction to its physical principles and applications*, Springer, 2019.

[57] D.J. Collins, R. O'Rorke, A. Neild, J. Han, Y. Ai, Acoustic fields and microfluidic patterning around embedded micro-structures subject to surface acoustic waves, *Soft Matter*, 15 (2019) 8691-8705.

[58] C. Devendran, T. Albrecht, J. Brenker, T. Alan, A. Neild, The importance of travelling wave components in standing surface acoustic wave (SSAW) systems, *Lab on a Chip*, 16 (2016) 3756-3766.

[59] M. Terada, S. Ide, T. Naito, N. Kimura, M. Matsusaki, N. Kaji, Label-Free Cancer Stem-like Cell Assay Conducted at a Single Cell Level Using Microfluidic Mechanotyping Devices, *Anal. Chem.*, 93 (2021) 14409-14416.

[60] Z. Li, P. Li, J. Xu, W. Shao, C. Yang, Y. Cui, Hydrodynamic flow cytometer performance enhancement by two-dimensional acoustic focusing, *Biomedical Microdevices*, 22 (2020) 1-12.

[61] R. Tao, W. Wang, J. Luo, S.A. Hasan, H. Torun, P. Canyelles-Pericas, J. Zhou, W. Xuan, M. Cooke, D. Gibson, Thin film flexible/bendable acoustic wave devices: Evolution, hybridization and decoupling of multiple acoustic wave modes, *Surface and Coatings Technology*, 357 (2019) 587-594.